
Article:
Punzo, G. orcid.org/0000-0003-4246-9045 (2022) An SIS network model with flow driven infection rates. Automatica, 137. 110107. ISSN 0005-1098

https://doi.org/10.1016/j.automatica.2021.110107

Automatica 137 (2022) 110107

Contents lists available at ScienceDirect

Automatica

journal homepage: www.elsevier.com/locate/automatica

Brief paper

An SIS network model with flow driven infection rates☆

Giuliano Punzo

Department of Automatic Control and Systems Engineering, The University of Sheffield, UK

ARTICLE INFO

Article history:
Received 20 January 2021
Received in revised form 8 July 2021
Accepted 28 September 2021
Available online xxxx

Keywords:
Epidemic spreading
SIS
Traffic-driven network

ABSTRACT

A flow-regulated infection rate is defined for a Susceptible-Infected-Susceptible (SIS) model revealing the network structural properties that influence the spread of infections. The infection rate is linked to the flow between compartments in the associated positive compartmental system, providing a self-regulatory effect on the spreading dynamics. This translates to infection carriers preferring to visit healthier sites over more infected ones. A flow-independent epidemic threshold is defined that sets the conditions on the graph's structure and the aggregate infection rate for a disease to either spread or die out. An individual-based mean-field approach returns results comparable to models with constant infection rates. This approach lends itself well to model the spread of infectious diseases as well as threats in IT networks, pharmacokinetics and the spread of disruptions on infrastructure networks.

1. Introduction

Epidemiological models have been proven valuable beyond the understanding of infectious diseases. They have been associated, for example, to the study of terrorist networks (Gutfraind, 2010), the spreading of rumors (Daley & Kendall, 1965) and computer viruses (Garetto, Gong, & Towsley, 2003).

Epidemic spreading is modelled considering that infected individuals infect the susceptible ones with whom they are in contact. The probability of contagion between an infected and a susceptible individual is the infection rate β, while recovery rate γ is the probability that an infected individual heals. In epidemic models, a contagion spreads successfully depending on a threshold, indicated by a basic reproduction number $\mathcal{R}_0$, which depends on the infection and recovery rates, and on the network of contacts, when this is considered (Nowzari, Preciado, & Pappas, 2016). An infection spreads throughout a population if $\mathcal{R}_0 > 1$ and dies out otherwise. An endemic state is achieved when all the nodes are infected. For constant and scalar infection and recovery rates, the basic reproduction number for the infection spreading on a network is $\beta\lambda_{max}(A)/\gamma$, where A is the graph adjacency matrix, and $\lambda_{max}(\cdot)$ indicates its largest eigenvalue in magnitude (Mei, Mohagheghi, Zampieri, & Bullo, 2017). The adjacency matrix is a square matrix of size N (the population's size), with entries indicating whether there is an interaction between the row- and the column-population member. A more formal definition is provided in Section 2.

Flow-driven networks (also called traffic-driven networks), which include transportation and IT systems, may present more complex contagion dynamics than those simply driven by static contact networks. For example, congestions and routing strategies change the epidemic threshold (Meloni, Arenas, & Moreno, 2009; Wu, Pu, Li, & Zhang, 2019). It is common to observe congestion on a road segment following disruptions on a parallel traffic route (Pregnolato, Ford, Wilkinson, & Dawson, 2017). Likewise, cascading failures of power networks are accelerated by the load transfer from disrupted sections of the network to the remaining, functional ones (Schäfer, Witthaut, Timme, & Latora, 2018). Pharmacokinetics focusses on understanding how drugs move from compartment to compartment of an organism (e.g. tissues or cells) depending on the target availability, to heal an infection as opposed to spreading it. When the drug binds to the targets, the availability of these decreases, i.e. the compartment gets healthier, and the drug accumulation reduces as a consequence (Mager & Jusko, 2001). This eventually provides a self-regulatory mechanism of the infection (or drug, as in the latter example) spreading.

Regulation of the spread dynamics (here the infection), has been empirically observed in the dynamics of invasive species and in relation to the Foot and Mouth animal disease (Arim, Abades, Neill, Lima, & Marquet, 2006). There, the change in the spreading rate is associated to a regulation effect, ultimately linked to a negative feedback on the infection rate, leading to a stable dynamics approaching asymptotic conditions.

☆ This work was partially supported by the EPSRC ENCORE Network+ (EP/N010019/1) Feasibility study fund. The material in this paper was not presented at any conference. This paper was recommended for publication in revised form by Associate Editor Vijay Gupta under the direction of Editor Christos G. Cassandras.

E-mail address: g.punzo@sheffield.ac.uk.

https://doi.org/10.1016/j.automatica.2021.110107

1.1. Contribution of this work

Spreading phenomena characterised by time-varying features of the system have been recently investigated through time-varying networks. Analytic results are only recently emerging (Gracy, Pare, Sandberg, & Johansson, 2020; Paré, Beck, & Nedić, 2018), yet this remains an open problem (Enright & Kao, 2018). In rare cases, the changes in the system characteristics have been modelled through a coupled dynamics, which would be particularly relevant for traffic-driven networks.

This work is therefore motivated by the challenge of modelling epidemic spreading with variable infection rate, in a way it can be expanded to flow-driven network systems. The question addressed here is *'how does the healthy/infected state of a node change the infection rate by altering the traffic flow in the network?'*. The heterogeneous mean field approach was previously considered to address this question by mapping the spreading dynamics to nodes grouped by degrees, therefore missing out on tracking the evolution of individual nodes (Meloni et al., 2009). More recent approaches considered a non-autonomous change of the infection characteristics or of the network structure (Gracy et al., 2020; Paré et al., 2018). In this work, instead, the loop is closed by linking the infection characteristics (i.e. the infection rate) to the traffic in the network and the dynamics of network traffic to the infectious state of the nodes. A Susceptible-Infected-Susceptible (SIS) model of infection spreading, where individuals can continuously get infected and heal, is coupled with a dynamical system (a so-called compartmental system) that captures the movement of infection carriers, which are assumed to prefer healthy nodes over more infected ones. This mimics a basic flow distribution scenario in traffic networks. Examples include the pharmacokinetic dynamics discussed earlier but also transportation networks where travellers tend to avoid already congested routes, leading to congest the other available routes as well.

This work takes a deterministic approach, as pioneered by Lajmanovich and Yorke (1976), where the Markov chain description of the infection dynamics is reduced through an individual mean field (Pagliara, Dey, & Leonard, 2018). This way, it retrieves and extends some of the results obtained for constant infection rates in works such as Fall, Iggidr, Sallet, and Tewa (2007), Khanafer, Başar, and Gharesifard (2016), Mei et al. (2017) and Mieghem, Omic, and Kooij (2009). As in Fall et al. (2007), the existence and stability of infection-free and endemic equilibrium points is established. As in Mieghem et al. (2009) an approximation of the system steady state at the endemic equilibrium is provided, but instead of using a recursive formula, the approximation is obtained in the limit for very high and very low infection rates as in Mei et al. (2017). Finally, results are obtained for simply connected graphs whereas the literature's main focus is on the strongly connected case only (e.g. Khanafer et al., 2016).

2. The model

In this work, the infection rate is a dynamic variable described through nodal load, with the load transfer rate from donor to receiver depending on the health of the receiving node. To this purpose, we define a graph $\mathcal{G} = \{\mathcal{V}, \mathcal{E}\}$ where $\mathcal{V} = \{1, 2 \dots N\}$ is a set of nodes and $\mathcal{E} \in \mathcal{V} \times \mathcal{V}$ is a set of ordered pairs of nodes, called edges. A *path* is an ordered sequence of vertices such that any pair of consecutive vertices in the sequence is an edge of the graph. A node is *globally reachable* if there exist a path from any other vertex to it. When a graph has a single globally reachable node, this is called a *sink*. The existence of a globally reachable node guarantees that the graph is *connected*, and vice-versa. If all nodes are globally reachable, the graph is said to be *strongly connected*. The graph adjacency matrix $A = [a_{ij}]$ is defined as $a_{ij} = 1$ if $(i, j) \in \mathcal{E}$, otherwise $a_{ij} = 0$. No self-loop are considered, hence $a_{ii} = 0\ \forall i$. A graph is said to be *balanced* if $(\mathbf{1}A)^T = A\mathbf{1}$.

A healthy node will receive flows from the neighbouring nodes. As the load accumulates in a node, its susceptibility to the infection increases. The incoming flows will reduce proportionally to the reduced health of the node. This corresponds to a donor-and-receptor controlled compartmental system (Jacquez & Simon, 1993). This setting is particularly relevant for systems such as IT networks or integrated transport networks, where routing and congestions play a major role. The network deterministic SIS model can be formulated in terms of the rate of the change of susceptible individuals $\dot{\mathbf{s}}$ and that of infected individuals $\dot{\mathbf{x}}$ (see for example Fall et al., 2007) as:

$$\begin{aligned} \dot{s}_i(t) &= -\beta_i s_i(t) \sum_{j \neq i} a_{ij} x_j(t) + \gamma x_i(t) \,, \\ \dot{x}_i(t) &= \beta_i s_i(t) \sum_{j \neq i} a_{ij} x_j(t) - \gamma x_i(t) \,. \end{aligned} \tag{1}$$

For a constant number of nodes, it is sufficient to consider the infected fraction, being this complementary to the susceptible part. Hence the second equation in (1) fully defines the SIS model.

The infection rate β_i in Eq. (1) is the probability that node i gets infected by any one of its neighbours at each iteration, while γ is the recovery rate for any node. While the recovery rate is a constant, the infection rate is a dynamic variable, i.e. $\beta_i = \beta_i(t)$, defined through a positive compartmental model (see Bullo, 2019, Ch. 10 and Jacquez & Simon, 1993). For such a model, with no flow to or from the environment, the dynamics can be expressed as:

$$\dot{\beta}_i(t) \triangleq \dot{q}_i(t) = -q_i(t) \sum_{j \neq i} f_{ij} + \sum_{j \neq i} f_{ji} q_j \,, \tag{2}$$

where $q_i(t)$ is the accumulated flow at node i at time t, which is set equal to the infection rate of node i, $\beta_i(t)$. The parameter f_{ij} is the flow constant on the edge from node i to node j, that is, the proportionality constant between $q_i(t)$ and its flow towards node j. The model is completed by setting the flow rates between nodes equal to the receivers' health. Dropping the explicit time dependence for a more simplified notation, this is expressed as $q_i \sum_{j \neq i} f_{ij} = \beta_i \sum_{j \neq i} a_{ij}(1 - x_j)$ and $\sum_{j \neq i} q_j f_{ji} = (1 - x_i) \sum_{j \neq i} a_{ji} \beta_j$ that is, the flow from node i to j depends on how infected node j is. The equations for the SIS system describing the unforced dynamics with load dependent infection rates are

$$\dot{x}_i = \beta_i (1 - x_i) \sum_{j \neq i} a_{ij} x_j - \gamma x_i \,, \tag{3}$$

$$\dot{\beta}_i = -\sum_{j \neq i} a_{ij} (1 - x_j) \beta_i + (1 - x_i) \sum_{j \neq i} a_{ji} \beta_j \,; \tag{4}$$

or in vector form

$$\dot{\mathbf{x}} = B(I - X)A\mathbf{x} - \gamma \mathbf{x} \,, \tag{5}$$

$$\dot{\boldsymbol{\beta}} = -BA(\mathbf{1} - \mathbf{x}) + (I - X)A^T \boldsymbol{\beta} \,, \tag{6}$$

where $B = \operatorname{diag}(\boldsymbol{\beta})$ and $X = \operatorname{diag}(\mathbf{x})$. Eq. (2) introduces the fundamental assumption of preferential movement of infection carriers from more infected to healthier nodes. This can be effectively pictured through a hydraulic network analogy, where water distributes according to the filling levels of the reservoirs (nodes). The water in the ith reservoir is replaced by the infection rate β_i, whose dynamics is described by Eq. (4). The flow constants, that could be thought of as the pipe diameters, are replaced by the health of the receiving nodes j to which node i is connected $(1 - x_j)$. Therefore, Eq. (4) is a balance equation for the infection rate β_i (water) shifting across nodes (reservoirs). The changes of the single nodes' infection rates are fed back onto the health of

the nodes through the infection dynamics in Eq. (3). This returns the regulatory effect previously discussed with reference to, for example, pharmacokinetics and network congestion problems. In its simplicity, this approach is a novelty in the modelling of infection dynamics.

In the remaining of the paper, unless otherwise specified, the graph will be considered simply connected.

3. Boundness and general solution for $\boldsymbol{\beta}$

The system in Eq. (5) has bounded trajectories in [0, 1] for the susceptible/infected state of each node, and bounded to positive values for the infection rate β. This is established in the following

Lemma 1. *The trajectories of* $\mathbf{x}$ *for the system in Eq. (5) are bounded to the hypercube of sides* $[0; 1]^N$ *for initial conditions within the hypercube. The trajectories of* $\boldsymbol{\beta}$ *are bounded to* $\mathbb{R}^N_{\geq 0}$ *for nonnegative initial conditions.*

Proof. Consider the value of $\dot{\mathbf{x}}$ on the boundary of the set. Eq. (3) yields $\dot{x}_i \geq 0$ when $x_i = 0$ and $\dot{x}_i \leq 0$ when $x_i = 1$. In particular, $\dot{x}_i = \beta_i \sum_{j \neq i} a_{ij} x_j \geq 0$ when $x_i = 0$ $\dot{x}_i = -\gamma$ when $x_i = 1$.

Similarly, $\boldsymbol{\beta}$ elements cannot take negative values as each element's derivative $\dot{\beta}_i$ is positive semidefinite for $\beta_i = 0$, as it can be seen immediately from Eq. (4).

The upper bound on β is provided by the conservation property defined in the following

Lemma 2. *The total infection rate for the system in Eq. (5) remains constant across the network.*

Proof. It is sufficient to prove that the net variation is null, that is $\mathbf{1}^T \dot{\boldsymbol{\beta}} = 0$, and indeed

$$\mathbf{1}^T \dot{\boldsymbol{\beta}} = \dot{\boldsymbol{\beta}}^T \mathbf{1} = -(\mathbf{1} - \mathbf{x})^T A^T B \mathbf{1} + \boldsymbol{\beta}^T A (I - X)\mathbf{1}$$
$$= -\sum_i \sum_j (1 - x_j) a_{ij} \beta_i + \sum_j \sum_i \beta_i a_{ij} (1 - x_j) = 0 \, .$$

A generalised solution for β is obtained next for which the graph Laplacian matrix, or simply the Laplacian L, is introduced as $L = D - A$, where D is a diagonal matrix with nonzero entries $d_{ii} = d_i = \sum_j^N a_{ij}$, corresponding to the nodal outdegree. The Laplacian has zero row sum and a null rightmost eigenvalue to which an eigenvector with all identical entries corresponds.

Lemma 3. *Let* $(\mathbf{x}^*, \boldsymbol{\beta}^*)$ *be an equilibrium point for the system in Eq. (5) and let* $\boldsymbol{\xi} = \mathbf{1} - \mathbf{x}^*$. *Then* $\boldsymbol{\beta}^* = \boldsymbol{\omega}$ *is the left eigenvector associated with the 0 eigenvalue of the Laplacian matrix obtained from the graph adjacency matrix* $A_\xi = A \, diag(\boldsymbol{\xi})$.

Proof. Eq. (6) is linear in β and can be written as

$$\dot{\boldsymbol{\beta}} = K_\xi \boldsymbol{\beta} \, , \tag{7}$$

where K_ξ is a matrix with diagonal elements equal to $-\sum_{j \neq i} a_{ij} \xi_j$, and off diagonal elements $a_{ji} \xi_i$, with $\xi_i = 1 - x_i$. It is evident that K_ξ is the transposed, negated Laplacian of a graph weighted by the value ξ of the edge end node. As such, it has a zero eigenvalue with multiplicity 1 corresponding to a right eigenvalue with positive entries. The Gershgorin circle theorem (Horn & Johnson, 1990, Ch. 6) guarantees that all the other eigenvalues have negative real part. $\boldsymbol{\beta}$ will hence converge to the right eigenvector corresponding to the zero eigenvalue of the matrix K_ξ. This holds, in particular, at equilibrium, that is for constant $\boldsymbol{\xi}$.

Lemma 1 guarantees that each node has a nonnegative infection value not greater than 1, hence the model is consistent with the phenomenon studied. The bound on the aggregate flow volume indicates that the model is particularly suitable for networked systems with null or balanced exchange with the environment.

4. Equilibrium points and stability in the infection-free state

In the infection-free state, the following result is obtained.

Theorem 1. *In a graph with more than one globally reachable node, the system in Eq. (5) has a unique infection-free equilibrium point:* $(\mathbf{x}^*, \boldsymbol{\beta}^*) = (\mathbf{0}, \hat{\beta} N \mathbf{w}_L)$; *where* $\mathbf{w}_L$ *is the left eigenvector of the graph Laplacian corresponding to the zero eigenvalue with unit* L_1 *norm and* $\hat{\beta} = \sum_i^N \beta_i(0)/N$. *Moreover,* $(\mathbf{x}^*, \boldsymbol{\beta}^*) = (\mathbf{0}, \hat{\beta}\mathbf{1})$ *if the graph is balanced,* $(\mathbf{x}^*, \boldsymbol{\beta}^*) = (\mathbf{0}, \mathbf{0})$ *for* $\boldsymbol{\beta}(0) = \mathbf{0}$. *The equilibrium point is asymptotically stable* if and only if $\frac{\hat{\beta} N \lambda_{max}(diag(\mathbf{w}_L)A)}{\gamma} < 1$.

Proof. First, note that $\mathbf{x} = \mathbf{0}$, the right hand side of Eq. (6) becomes $-BA\mathbf{1} + A^T \boldsymbol{\beta}$. Therefore:

$$\dot{\boldsymbol{\beta}} = -BA\mathbf{1} + A^T \boldsymbol{\beta} = -B\mathbf{d} + A^T \boldsymbol{\beta} = -D\boldsymbol{\beta} + A^T \boldsymbol{\beta}$$
$$= -L^T \boldsymbol{\beta} \, . \tag{8}$$

The left hand side is null for $\boldsymbol{\beta} = \mathbf{0}$ or for $\boldsymbol{\beta} = \mathbf{w}_L$, meaning that any vector parallel to the eigenvector $\mathbf{w}_L$ would be an equilibrium for $\boldsymbol{\beta}$. This is also obtainable from Lemma 3 for $\mathbf{x} = \mathbf{0}$. The actual expression $(\mathbf{0}, \boldsymbol{\beta}^*) = (\mathbf{0}, \hat{\beta} N \mathbf{w}_L)$ is guaranteed by the conservation of the total infection rate through Lemma 2.

To prove that the infection-free equilibrium is asymptotically stable, consider the coordinate transformation $\bar{\mathbf{x}} = \mathbf{x}$, $\bar{\boldsymbol{\beta}} = \boldsymbol{\beta} - \hat{\beta} N \mathbf{w}_L$ and the Lyapunov function $V(\bar{\mathbf{x}}) = \frac{1}{2} \bar{\mathbf{x}}^T \bar{\mathbf{x}}$. In the new coordinates, the origin is a stable equilibrium point. The time derivative yields

$$\dot{V}(\bar{\mathbf{x}}, \bar{\boldsymbol{\beta}}) = \bar{\mathbf{x}}^T diag(\bar{\boldsymbol{\beta}} + \hat{\beta} N \mathbf{w}_L)(I - \bar{X})A\bar{\mathbf{x}} - \bar{\mathbf{x}}^T \gamma \bar{\mathbf{x}}$$
$$\leq \bar{\mathbf{x}}^T diag(\bar{\boldsymbol{\beta}} + \hat{\beta} N \mathbf{w}_L) A \bar{\mathbf{x}} - \bar{\mathbf{x}}^T \gamma \bar{\mathbf{x}} \, ,$$

where $\bar{X} = diag(\bar{\mathbf{x}})$. The condition for $\dot{V} \leq 0$ is then $\lambda_{max} diag(\bar{\boldsymbol{\beta}} + \hat{\beta} N \mathbf{w}_L) A \leq \gamma$. Note that $\boldsymbol{\beta}$ must satisfy Lemmas 1 and 2, therefore $\mathbf{1}^T(\bar{\boldsymbol{\beta}} + \hat{\beta} N \mathbf{w}_L) = \hat{\beta} N$ implies $\bar{\boldsymbol{\beta}} = \mathbf{0}$. This makes the Lyapunov function negative semidefinite if $\hat{\beta} N \lambda_{max}(diag(\mathbf{w}_L)A) \leq \gamma$. The derivative is only negative semidefinite as the equality is satisfied for any value of $\boldsymbol{\beta}$. Using the La Salle–Krasovskii theorem (Khalil, 2002, Ch. 4), however, it can be seen that the equilibrium is asymptotically stable as the solution set for which $\dot{V} = 0$ reduces to $(\mathbf{0}, \hat{\beta} N \mathbf{w}_L)$. It is sufficient to note that the trajectories of the systems confined to $\mathbf{x} = \mathbf{0}$ must satisfy Eq. (8), that together with Lemma 2 proves the theorem. It is moreover easy to verify that the Jacobian of the system, obtained linearising at the infection-free equilibrium point, has all the eigenvalue in the closed left plane only for $\frac{\hat{\beta} N \lambda_{max}(diag(\mathbf{w}_L)A)}{\gamma} \leq 1$.

Remark 1. The equilibrium point $(\mathbf{0}, \mathbf{0})$ is a special case of the infection-free equilibrium, that, because of the conservation of $\boldsymbol{\beta}$, is only achievable for identically null initial conditions.

Remark 2. In case of a single globally reachable node, i.e. a sink, the left eigenvector of the graph Laplacian has a single nonzero entry, corresponding to such a node. If this is node i, then $a_{ij} = 0 \; \forall \; j$ and the only nonzero element of $\mathbf{w}_L$ is its ith element. This means that, the infection free equilibrium is always asymptotically stable, for any value of $\hat{\beta} N$ for $\gamma > 0$. The particular expression for the equilibrium point becomes $(\mathbf{x}^*, \boldsymbol{\beta}^*) = (\mathbf{0}, \boldsymbol{\beta}_s)$,

where $\boldsymbol{\beta}_s = [0, \ldots, 0, \hat{\beta}N, 0, \ldots, 0]^T \in \mathbb{R}^N$, that is a vector where the only nonzero component $\hat{\beta}N$ corresponds to the sink node. This and $(\mathbf{x}^*, \boldsymbol{\beta}^*) = (\mathbf{0}, \hat{\beta}\mathbf{1})$ derive from the property of the eigenvector corresponding to the zero eigenvalue of the Laplacian matrix, where nonzero entries correspond to globally reachable nodes (Punzo, Young, Macdonald, & Leonard, 2016).

The stability analysis highlights the conditions that make the infection-free equilibrium unstable making the system unable to dissipate the infection before it spreads. These map to network characteristics, recovery rate and total infection rate. As the equilibrium $(\mathbf{0}, N\hat{\beta}\mathbf{w}_L)$ is stable for $\gamma \geq \hat{\beta}N\lambda_{max}(diag(\mathbf{w}_L)A)$ and unstable otherwise, the epidemic threshold, which is a function of the network structure, the recovery rate and the initial conditions can be defined as

$$\mathcal{R}_\beta \triangleq \frac{\hat{\beta}N\lambda_{max}(diag(\mathbf{w}_L)A)}{\gamma} . \tag{9}$$

$\mathcal{R}_\beta = 1$ is the critical threshold. For $\mathcal{R}_\beta < 1$ the system converges to an infection-free equilibrium while for $\mathcal{R}_\beta > 1$ the infection will spread through the network.

5. Behaviour above the threshold

The equilibrium in the endemic state is not immediately recoverable by inspection of Eq. (5) and (6), with the exception of balanced, degree-regular graphs, as detailed later. Moreover, an endemic equilibrium, is only achievable in strongly connected graphs, as it will be shown next together with the system's stability and approximated equilibrium expressions above the threshold.

5.1. Stability of the equilibrium above the threshold

The stability of the endemic equilibrium is here analysed for simply connected graph, leveraging and extending (Khanafer et al., 2016) through the new model.

Theorem 2. *For $\mathcal{R}_\beta > 1$ the equilibrium for the system in Eq. (5) and (6) is globally asymptotically stable. Moreover, an endemic equilibrium can only be achieved in the strongly connected component of the graph.*

Proof. Consider Eq. (5) and define $\tilde{\mathbf{x}} = \mathbf{x} - \mathbf{x}^*$ that is the difference between the state $\mathbf{x}$ and the equilibrium. Then

$$\begin{aligned}\dot{\tilde{\mathbf{x}}} + \dot{\mathbf{x}}^* &= B\left(I - \tilde{X} - X^*\right)A(\tilde{\mathbf{x}} + \mathbf{x}^*) - \Gamma(\tilde{\mathbf{x}} + \mathbf{x}^*) \\ &= \Lambda(\mathbf{x}^*)\mathbf{x}^* + \Lambda(\mathbf{x}^*)\tilde{\mathbf{x}} - B\tilde{X}A\mathbf{x} ,\end{aligned} \tag{10}$$

where $\Gamma = \gamma I$ and $\Lambda(\mathbf{x}^*) = B[I - X^*]A - \Gamma$. Note that $\Lambda(\mathbf{x}^*)$ is a Metzler matrix as all its off-diagonal elements are nonnegative.

First, consider a strongly connected graph for which A is irreducible, which makes $\Lambda(\mathbf{x}^*)$ irreducible too (Khanafer et al., 2016). At equilibrium, it holds $\Lambda(\mathbf{x}^*)\mathbf{x}^* = \mathbf{0}$, hence $\mathbf{x}^*$ is the eigenvector corresponding to the zero eigenvalue of $\Lambda(\mathbf{x}^*)$ and because all entries of $\mathbf{x}^*$ are positive and $\Lambda(\mathbf{x}^*)$ is irreducible, the Perron–Frobenius theorem (Farina & Rinaldi, 2000) guarantees that $\mathbf{x}^*$ is the Frobenius vector of $\Lambda(\mathbf{x}^*)$ corresponding to the zero eigenvalue. All the other eigenvalues are negative, hence $\Lambda(\mathbf{x}^*)$ is negative semidefinite. It follows that $\exists R \in \mathbb{R}^{N\times N}$ diagonal and positive, such that $\Lambda(\mathbf{x}^*)^T R + R\Lambda(\mathbf{x}^*)$ is negative semidefinite. Consider the Lyapunov function $V(\tilde{\mathbf{x}}) = \tilde{\mathbf{x}}^T R\tilde{\mathbf{x}}$.

$$\begin{aligned}\frac{dV(\tilde{\mathbf{x}})}{dt} &= \frac{dV}{d\tilde{\mathbf{x}}}\frac{d\tilde{\mathbf{x}}}{dt} = \frac{d}{d\tilde{\mathbf{x}}}(\tilde{\mathbf{x}}^T R\tilde{\mathbf{x}})\left(\Lambda(\mathbf{x}^*)\tilde{\mathbf{x}} - B\tilde{X}A\mathbf{x}\right) \\ &= \tilde{\mathbf{x}}^T\left(\Lambda(\mathbf{x}^*)^T R + R\Lambda(\mathbf{x}^*)\right)\tilde{\mathbf{x}} - 2\tilde{\mathbf{x}}^T RB\tilde{X}A\mathbf{x} \\ &\leq -2\tilde{\mathbf{x}}^T RB\tilde{X}Ax = -2\tilde{\mathbf{x}}^T\tilde{X}RBA\mathbf{x} .\end{aligned} \tag{11}$$

The last equality holds as diagonal matrices commute. Because R, B and A are positive semidefinite, and because the elements of $\mathbf{x}$ are nonnegative, it can be concluded that the right hand side is negative semidefinite. The first part of the proof is concluded noting that for $\mathcal{R}_\beta > 1$ $\mathbf{x} = \mathbf{0}$ is unstable. Note that no assumptions are made about B other than having positive diagonal entries (as per Lemma 3 and the strong connectivity).

Consider now a simply connected graph, where a subset of nodes are not globally reachable. Without loss of generality, assume that the first n nodes are not globally reachable and the remaining $m = N - n$ belong to the strongly connected component of the graph. Such a graph has an adjacency matrix with an all-zero lower-left partition with m rows and n columns. Eq. (7), Lemma 3, Remark 2 and Punzo et al. (2016), guarantee that, at equilibrium, the first n elements of $\boldsymbol{\beta}^*$ are null. Therefore, from Eq. (5), the equilibrium for $\mathbf{x}$ is $\mathbf{x}^* = \left[0, \ldots .0, x^*_{n+1} \ldots x^*_m\right]^T$. The all-zero lower-left partition of A is found in $\Lambda(\mathbf{x}^*)$ as well, meaning that the spectrum of $\Lambda(\mathbf{x}^*)$ is the union of its upper-left and lower-right partitions' spectra. The first n rows and column of $\Lambda(\mathbf{x}^*)$ form a diagonal matrix $-\gamma I_n$, hence $\Lambda(\mathbf{x}^*)\mathbf{x}^* = \mathbf{0}$ implies that that the zero eigenvalue belongs to the lower-right partition, which describes the dynamics of the strongly connected component. The corresponding eigenvector of $\Lambda(\mathbf{x}^*)$ has the first n entries null and the last m entries positive. As $\Lambda(\mathbf{x}^*)$ is still negative semidefinite, the proof can be completed as in the strongly connected case and is here omitted for brevity.

Proving the stability above the threshold means that once the conditions in terms of γ, network structure and total infection rate support the infection spreading, this achieves a steady value for each node, i.e. an asymptotically stable equilibrium. Although this work cannot offer a general expression for such an equilibrium, approximate expressions are offered next.

5.2. Endemic equilibrium

Approximated expressions are here provided for very high and very low levels of infection considering just the strongly connected case, as the endemic equilibrium can only be achieved in the strongly connected component of any graph. These approximations leverage (Mei et al., 2017), and the newly proposed epidemic threshold (9).

Define λ_{BA} as the largest eigenvalue of $diag(\mathbf{w}_L)A$. Let $\mathbf{v}_{BA}$ and $\mathbf{w}_{BA}$ being the corresponding right and left eigenvectors. Note that $\mathbf{v}_{BA}$ and $\mathbf{w}_{BA}$ are also eigenvectors of $\hat{\beta}Ndiag(\mathbf{w}_L)A$ corresponding to the eigenvalue $\lambda_{BA} \triangleq \hat{\beta}N\lambda_{BA}$. In order to simplify the notation, define $V \triangleq diag(\mathbf{v}_{BA})$, $\tilde{\boldsymbol{\beta}} \triangleq N\hat{\beta}\mathbf{w}_L$ and $\tilde{B} \triangleq diag(\tilde{\boldsymbol{\beta}})$. It is now possible to state the following result.

Theorem 3. *For a strongly connected graph, the infection in the nodes in the endemic state equilibrium for the system (5)–(6) can be approximated as*

- $\boldsymbol{\zeta} \triangleq \mathbf{x}^* + \boldsymbol{\eta} = \alpha\mathbf{v}_{BA}$ *for* $\lambda_{BA}/\gamma - 1 \to 0^+$,
- $\boldsymbol{\chi} \triangleq \mathbf{x}^* + \mathbf{e} = \mathbb{1} - \gamma\ B^{*-1}\ D^{-1}\mathbb{1}$ *for* $\max_i \gamma/\beta_i \to 0^+$,

where the equilibrium value for $\boldsymbol{\beta}$ is $\tilde{\boldsymbol{\beta}} \triangleq \boldsymbol{\beta}^* = \hat{\beta}N\mathbf{w}_L$ and α is a constant equal to $\alpha = \frac{\lambda_{BA}-\gamma}{\lambda_{BA}}\frac{\mathbf{w}_{BA}^T\mathbf{v}_{BA}}{\mathbf{w}_{BA}^T V\mathbf{v}_{BA}}$. The error vectors $\boldsymbol{\eta}$ and $\mathbf{e}$ have elements $\eta_i = \mathcal{O}\left(\frac{((\lambda_{BA}-\gamma)(I-\Omega\,\mathrm{diag}(\mathbf{v}_{BA}))\boldsymbol{\zeta})_i}{\min_i g_i}\right)$, $e_i = \mathcal{O}\left(\frac{(\gamma\lambda_{L^S}\boldsymbol{\chi})_i}{\min_i h_i}\right)$, λ_{L^S} is the largest eigenvalue in magnitude of the scaled Laplacian L^S which has each row scaled by the node outdegree; $\Omega = \alpha\frac{\lambda_{BA}}{\lambda_{BA}-\gamma} = \frac{\mathbf{w}_{BA}^T\mathbf{v}_{BA}}{\mathbf{w}_{BA}^T V\mathbf{v}_{BA}}$. $g_i = \|-\lambda_{BA}\zeta_i - \gamma + (1-\alpha v_{BAi})\tilde{\beta}_i d_i\|$ and $h_i = \|\tilde{\beta}_i d_i - \tilde{\beta}_i\gamma\sum_j \frac{a_{ij}}{\tilde{\beta}_j d_j}\|$.

Proof. At equilibrium, Eq. (5) yields

$$\dot{\mathbf{x}} = B(I - X)A\mathbf{x} - \gamma\mathbf{x} = (I - X)BA\mathbf{x} - \gamma\mathbf{x} = 0 \tag{12}$$

as the diagonal matrix product is commutable. Note that $\lambda_{BA}/\gamma - 1 \to 0^+$ implies that $\mathcal{R}_\beta$ is only marginally larger than unity, hence the elements of $\mathbf{x}$ will be positive but much smaller than 1. Eq. (12) then yields $diag(\boldsymbol{\beta}^*)A\mathbf{x}^* \approx \gamma\mathbf{x}^*$, that is, as $\mathbf{x}^*$ gets smaller, the equation resembles an eigenvalue-eigenvector problem. It is then possible to consider $\alpha\mathbf{v}_{BA}$ as an approximate solution. Substituting it in the last equality of Eq. (12) yields

$$\begin{aligned}
&\tilde{B}A\alpha\mathbf{v}_{BA} - \tilde{B}\alpha^2 VA\mathbf{v}_{BA} - \gamma\alpha\mathbf{v}_{BA} = 0\ ,\\
&\therefore \lambda_{BA}\mathbf{v}_{BA} - \alpha\lambda_{BA}V\mathbf{v}_{BA} - \gamma\mathbf{v}_{BA} = 0\ ,\\
&\therefore (\lambda_{BA} - \gamma)\mathbf{v}_{BA} = \alpha\lambda_{BA}diag(\mathbf{v}_{BA})\mathbf{v}_{BA}
\end{aligned} \tag{13}$$

The first part of the theorem is proved by pre-multiplying both sides by $\mathbf{w}_{BA}^T$, which yields α. Note that for $\lambda_{BA}/\gamma - 1 \to 0^+$, $\lambda_{BA}/\gamma \to 1$, hence $\alpha \to 0^+$, which confirms the approximate equilibrium is characterised by a small value of the infection.

For the second part of the theorem, note that if $\max_i \gamma/\tilde{\beta}_i \to 0^+$, then also $\max_i \gamma/(\tilde{\beta}_i d_i) \to 0^+$ as $d_i \geq 1\ \forall\, i$ (strong connectivity). Consider now the first of Eq. (3) and its approximate solution $\boldsymbol{\chi}$. Substituting the values for χ_i, it yields the residual dynamics $\epsilon_i = (\gamma/d_i)\sum_{j\neq i} a_{ij}\left(1 - \gamma/(\tilde{\beta}_j d_j)\right) - \gamma\left(1 - \gamma/(\tilde{\beta}_i d_i)\right)$, which in vector form becomes

$$-\gamma D^{-1}L\boldsymbol{\chi} = -\gamma L^s\boldsymbol{\chi} = \boldsymbol{\epsilon}. \tag{14}$$

Strong connectivity guarantees that D is not singular and $L^s \triangleq D^{-1}L$ is a scaled Laplacian with diagonal entries equal to 1. The eigenvalues of the scaled Laplacian L^s in Eq. (14) are confined between 0 and 2 by Gershgorin. In particular, for $\gamma \leq 0.5$ the spectrum of γL^s is confined between 0 and 1, ensuring that the right hand side is "smaller" than $\boldsymbol{\chi}$. For the Laplacian's properties (Section 3), if $\boldsymbol{\chi} \in span\{\mathbf{1}\}$, then the residuals are null.

For the approximation errors $\boldsymbol{\eta}$ and $\mathbf{e}$, first it is shown that the residual dynamics is "small", which justifies to consider a linearised approach to obtain the difference between the approximate expressions and the exact equilibrium. Consider $\mathbf{x} = \boldsymbol{\zeta} = \alpha\mathbf{v}_{BA}$ in Eq. (5) and define the remainder $\mathbf{r}$ as the residual dynamics,

$$\begin{aligned}
\mathbf{r} =& [I - \alpha V]\tilde{B}A\alpha\mathbf{v}_{BA} - \gamma\alpha\mathbf{v}_{BA}\\
=& \Omega\frac{(\lambda_{BA} - \gamma)^2}{\lambda_{BA}}\mathbf{v}_{BA} - \Omega^2\frac{(\lambda_{BA} - \gamma)^2}{\lambda_{BA}}V\mathbf{v}_{BA}\\
=& \Omega\frac{(\lambda_{BA} - \gamma)^2}{\lambda_{BA}}(I - \Omega V)\mathbf{v}_{BA} = (\lambda_{BA} - \gamma)(I - \Omega V)\boldsymbol{\zeta}
\end{aligned} \tag{15}$$

Clearly, $\mathbf{r} \to \mathbf{0}$ as long as $\lambda_{BA} - \gamma \to 0^+$, as per the hypothesis. The Jacobian at $\boldsymbol{\zeta}$ is $J(\boldsymbol{\zeta}) = \tilde{B}(I - \alpha V)A - \alpha\tilde{B}\ diag(A\mathbf{v}_{BA}) - \gamma I$. Because $\tilde{B}\ diag(A\mathbf{v}_{BA}) = diag(\tilde{B}A\mathbf{v}_{BA}) = \lambda V$, then $J(\boldsymbol{\zeta}) = (I - \alpha V)\tilde{B}A - \alpha\lambda_{BA}V - \gamma I$, where the off-diagonal elements of row i sum to $(1 - \alpha v_{BAi})\tilde{\beta}_i d_i$ and the diagonal element is $-\alpha\lambda_{BA}v_{BAi} - \gamma$. Through the Gershgorin disk, the lower bound for magnitude of the largest eigenvalue of $J(\boldsymbol{\chi})$ is

$$\begin{aligned}
\|\lambda_{max}(J(\boldsymbol{\zeta}))\| &\geq \min_i \|-\lambda_{BA}\zeta_i - \gamma + (1 - \alpha v_{BAi})\tilde{\beta}_i d_i\|\\
&= \min_i g_i.
\end{aligned} \tag{16}$$

Consider now the error $\mathbf{e} = \boldsymbol{\chi} - \mathbf{x}$ and the limit to the residual dynamics from Eq. (14). The Jacobian at $\boldsymbol{\chi}$ is: $J(\boldsymbol{\chi}) = \gamma D^{-1}A - \tilde{B}\ diag\{[A(I - \gamma D^{-1}\tilde{B}^{-1})]\mathbf{1}\} - \gamma I$ $J(\chi)$ is diagonally dominated provided that $\gamma/(\beta_j d_j) \leq 1$. This is actually the case as, for χ_j to be a meaningful approximation of x_j, it must be $0 \leq \chi_j \leq 1$.

It can be concluded that the magnitude of the largest eigenvalue of $J(\boldsymbol{\chi})$ is bounded from below by

$$\begin{aligned}
&\|\lambda_{max}(J(\boldsymbol{\chi}))\| \geq \min_i \|-\tilde{\beta}_i\sum_{j\neq i} a_{ij}\left(1 - \frac{\gamma}{\tilde{\beta}_j d_j}\right)\|\\
&= \min_i \|-\tilde{\beta}_i d_i + \gamma\tilde{\beta}_i\sum_{j\neq i}\frac{a_{ij}}{\tilde{\beta}_j d_j}\| = \min_i h_i\ .
\end{aligned} \tag{17}$$

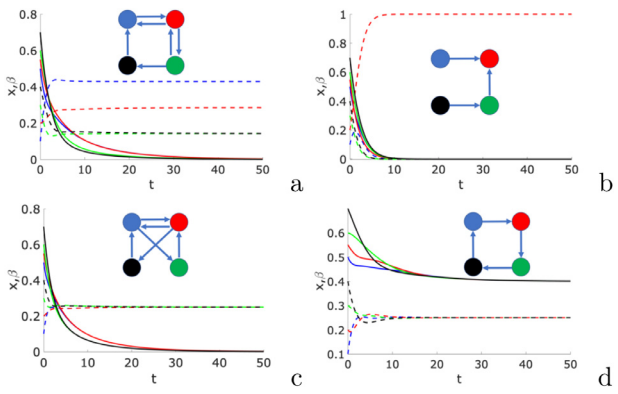

Fig. 1. Examples of equilibrium points on 4 node graphs. Solid and dashed lines correspond to x and β dynamics respectively (a): Generic graph, below the threshold. (b): Sink, below the threshold. (c): Balanced graph, below the threshold. (d): Balanced with constant degree, above the threshold.

These approximate solutions hold for the strongly connected component of any graph. For the not globally reachable nodes, the value of $\boldsymbol{\chi}$ is zero, as proved. The quantifiable errors ensure the model's predictive abilities in both the infection-free and the endemic states.

5.3. Equilibrium at consensus, a special case

In the case of a balanced graph with constant degree, the left and right eigenvectors of the adjacency matrix and of the Laplacian corresponding to λ_{max} are both $\in$ span$\{\mathbf{1}\}$. Considering Eq. (5), $\boldsymbol{\beta} \in$ span$\{\mathbf{1}\}$ implies $\mathbf{x}$ to be either $\mathbf{0}$ or $[1 - \gamma/(\hat{\beta}d)]\mathbf{1}$, where d is the (uniform) degree of the graph and also the dominant eigenvalue of the adjacency matrix. The linearisation at the equilibrium point $(\mathbf{x}^*, \boldsymbol{\beta}^*) = (\frac{\hat{\beta}d-\gamma}{\hat{\beta}d}\mathbf{1}, \hat{\beta}\mathbf{1})$ yields

$$J_{\left(\frac{\hat{\beta}d-\gamma}{\hat{\beta}d}\mathbf{1},\hat{\beta}\mathbf{1}\right)} = \left[\begin{array}{c|c} -\hat{\beta}\left(\frac{\hat{\beta}d-\gamma}{\hat{\beta}d}\mathcal{L} - A\right) - \gamma I & \frac{\gamma}{\hat{\beta}}\left(\frac{\hat{\beta}d-\gamma}{\hat{\beta}d}\right)I \\ \hline -\hat{\beta}\mathcal{L} & -\frac{\gamma}{\hat{\beta}d}\mathcal{L}^T \end{array}\right].$$

The first N rows define N identical Gershgorin circles centred at $-\hat{\beta}\left(\frac{\hat{\beta}d-\gamma}{\hat{\beta}d}\right)d - \gamma$. It is easy to verify, and here omitted for brevity, that for $\mathcal{R}_\beta > 1$, these Gershgorin circles are all contained in the left open plane. In this special case, the epidemic threshold reduces to $\hat{\beta} \geq \frac{\gamma}{\lambda_{max}(A)} = \frac{\gamma}{d}$, as in Mei et al. (2017). Fig. 1 shows the behaviour of the system converging to the infection free and endemic equilibria for different 4-node graphs.

6. Numerical simulations

Numerical simulations are provided by integrating numerically Eqs. (5) and (6) for two 5-node graphs, for the London urban railway system and the US Western power grid.

6.1. 5-Node graphs

The system (5)–(6) has been integrated numerically for connected and strongly connected, 5-node graphs (Fig. 2) with initial conditions $(\mathbf{x}(0), \boldsymbol{\beta}(0))$ selected from uniform distributions over the interval $[0, 1]$, imposing $\sum_i \beta_i(0) = 1$. The value of critical threshold is achieved for $\gamma = \lambda_{BA} = 0.3965$ for the connected graph and $\gamma = \lambda_{BA} = 0.3965$ for the fully connected graph. γ was then altered to produce a behaviour, slightly above ($\mathcal{R}_\beta = 1.01$), and well above the threshold ($\mathcal{R}_\beta = 20$).

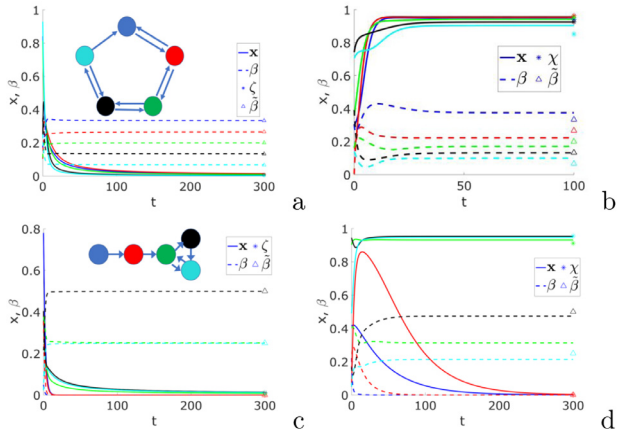

Fig. 2. Behaviour slightly above the threshold $\mathcal{R}_\beta = 1.01$ (a,c) and well above the threshold $\mathcal{R}_\beta = 20$. (b,d) for a 5 node strongly connected network (a,b) and a simply connected one (c,d) with $\sum_i(\beta_i(0)) = 1$ in all cases. The $\tilde{\beta}$ markers △ for the cyan and green nodes are superimposed in panes c and d.

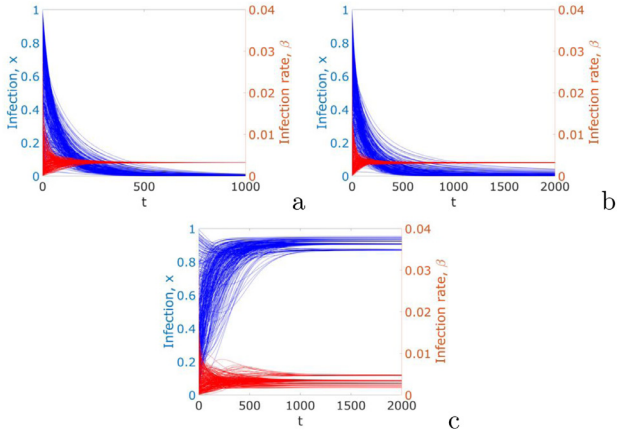

Fig. 3. Threshold behaviour for the London railway system network (a) behaviour below the threshold ($\mathcal{R}_\beta = 0.8$, $\gamma = 0.0159$). (b) behaviour slightly above the threshold ($\mathcal{R}_\beta = 1.01$, $\gamma = 0.0126$). (c) behaviour highly above the threshold ($\mathcal{R}_\beta = 20$, $\gamma = 6.34 \times 10^{-4}$).

Table 1
The approximate solutions $\boldsymbol{\zeta}$ and $\boldsymbol{\chi}$, and $\tilde{\boldsymbol{\beta}} = \hat{\beta}N\mathbf{w}_L$ from Theorem 3 are compared to the result of the numerical simulations through the root mean square error (RMS).

		RMS error	
Nodes	$\mathcal{R}_\beta$	$\boldsymbol{\zeta}$ or $\boldsymbol{\chi}$	$\tilde{\boldsymbol{\beta}} = \hat{\beta}N\mathbf{w}_L$
5	1.01	$3.37e^{-4}$	$4.87e^{-4}$
	20	$2.42e^{-2}$	$3.35e^{-2}$
301	1.01	$5.16e^{-3}$	$2.35e^{-5}$
	20	$1.98e^{-2}$	$5.67e^{-4}$
1722	1.01	$9.5e^{-4}$	$4.77e^{-6}$
	20	$4.4e^{-2}$	$1.60e^{-4}$

6.2. Infrastructure networks

The model is applied to the London railway system (De Domenico, Solé-Ribalta, Gómez, & Arenas, 2014), and to the US Western powergrid network (Rossi & Ahmed, 2015), which are both undirected. For the London urban railway network ($N = 301$), the initial conditions for $\boldsymbol{\beta}$ are set equal to the 2015 daily average passenger counts per station (Transport for London, 2021), p_i, scaled so that $\sum_i p_i = \sum_i \beta_i(0) = 1$ for $i = 1, 2 \dots N$. The initial conditions $\mathbf{x}(0)$ are selected at random in $[0, 1]^N$. The critical threshold is obtained for $\gamma = \lambda_{BA} = 0.0127$. Fig. 3 shows the results for the dynamics below the threshold ($\mathcal{R}_\beta = 0.8$), slightly above the threshold ($\mathcal{R}_\beta = 1.01$), and well above the threshold ($\mathcal{R}_\beta = 20$). In the appendix, it is shown that the model can rank stations and lines more likely to suffer disruptions, comparing real and simulated results through the Kendall-τ coefficient. For the US Western powergrid network, the giant connected component was considered ($N = 1722$). Random initial conditions for β are set, scaled so that $\sum_i p_i = \sum_i \beta_i(0) = \beta_i(t) = 1$ for $i = 1, 2 \dots N$. The initial conditions $\mathbf{x}(0)$ are selected at random as in the London railway system. For such a network and choice of $\boldsymbol{\beta}$, the critical threshold is obtained for $\gamma = \lambda_{BA} = 0.00289$. This network was simulated for $\mathcal{R}_\beta = 1.01$ and for $\mathcal{R}_\beta = 20$). The approximated equilibria and the simulation output were compared through the mean square errors in Table 1 for all the strongly connected networks considered, showing good agreement.

7. Conclusions

This work proposed a novel SIS model with dynamic infection rate, relevant to flow driven networks where self-regulatory mechanisms are often present, including engineering and biological systems. The infection-free equilibrium was exactly computed. Approximate expressions were provided for the equilibrium above the threshold in strongly connected components of graphs, an exact one for balanced graphs with constant degree and for the non globally-reachable nodes. The stability of the equilibria was analysed and related to the epidemic threshold, with numerical simulations supporting the results.

Preserving the aggregate infection rate, which represents the total network's traffic volume, derives from the compartmental system modelling choice. This hypothesis, is key to obtain analytic results comparable and beyond models featuring a constant infection rate.

The epidemic threshold links the network structure to the total flow volume. By looking at the epidemic threshold in Eq. (9), whether a disease spreads or dies out depends on the total infection rate ($\hat{\beta}N$), the network topology ($\lambda_{max}(diag(\mathbf{w}_L)A)$) and the nodes' recovery ability (γ). It can be concluded that flow-driven networks are more resistant against infectious spreading if the structure minimises the largest eigenvalue of the matrix $diag(\mathbf{w}_L)A$. This threshold is in agreement with the literature as it reduces to the one in Fall et al. (2007) and Khanafer et al. (2016) for constant infection rate. While in general, there is no closed form expression for the spectral radius of a matrix, higher degrees and link densities are associated with higher values of the spectral radius (Mieghem et al., 2009), which is the present case too.

Acknowledgments

The author acknowledges the discussion and the intellectual contribution by Prof. Dario Bauso in the early stages of the work, as well as the fruitful discussion with Dr Iñaki Esnaola.

Appendix. Comparison with excess journey time on the London underground lines

The London urban railway system includes several subnetworks, which share a number of stations. Transport for London (TFL) publishes yearly figures of daily average of passengers' inflow and outflow per station for the London underground, the Overground and the Dockland Light Railway (DLR) (Transport for London, 2021). Excess journey time (EJT) per line (a measure of delay) is also available as a network performance indicator for the London underground, although figures are available across

2015 EJT ranking	3 most disrupted stations	15 most disrupted stations	30 most disrupted stations
1 Circle	District	Piccadilly	District
2 Central	Piccadilly	Metropolitan	Piccadilly
3 Metropolitan	Metropolitan	District	Northern
4 District	Circle	Northern	Circle
5 Piccadilly	Central	Circle	Metropolitan
6 Victoria	Victoria	Jubilee	Central
7 Northern	Northern	Central	Jubilee
8 Jubilee	Jubilee	Bakerloo	Victoria
9 Bakerloo	Bakerloo	Waterloo	Waterloo
10 Waterloo	Waterloo	Victoria	Bakerloo
Kendall-τ coeff.	0.6444	0.3333	0.4222
p-value	0.0091	0.2164	0.1083

Fig. A.1. Comparison of the ranking of the most delayed lines in the London underground, according to the extra journey time (EJT), in the year 2014/15 with the ranking from the simulations above the threshold. The passenger loads per station are extracted from the 2015 average daily inflows per station. Blue-cold colours correspond to lines that have accumulated the higher delays. The simulations award 1 point to the top 3, 15 and 30 most infected station, that are summed up to the line they belong. Lines from Central to Waterloo never appear when the 3 most affected stations only are considered and are therefore shaded with the same colour, having all null score. The Kendall-τ coefficient and associated p-value are reported at the bottom.

2016 EJT ranking	3 most disrupted stations	15 most disrupted stations	30 most disrupted stations
1 Circle	District	Piccadilly	District
2 Central	Piccadilly	Metropolitan	Northern
3 District	Circle	Northern	Piccadilly
4 Piccadilly	Metropolitan	District	Circle
5 Bakerloo	Central	Circle	Metropolitan
6 Northern	Bakerloo	Jubilee	Central
7 Metropolitan	Northern	Central	Jubilee
8 Victoria	Victoria	Bakerloo	Victoria
9 Jubilee	Jubilee	Waterloo	Bakerloo
10 Waterloo	Waterloo	Victoria	Waterloo
Kendall-τ coeff.	0.6889	0.2	0.4222
p-value	0.0047	0.4843	0.1083

Fig. A.2. Comparison of the ranking of the most delayed lines in the London underground, according to the extra journey time (EJT), in the year 2015/16 with the ranking from the simulations above the threshold. The passenger loads per station are extracted from the 2016 average daily inflows per station. Blue-cold colours correspond to lines that have accumulated the higher delays. The simulations award 1 point to the top 3, 15 and 30 most infected station, that are summed up to the line they belong. Lines from Central to Waterloo never appear when the 3 most affected stations only are considered and are therefore shaded with the same colour, having all null score. The Kendall-τ coefficient and associated p-value are reported at the bottom.

the years, as opposed than per solar year. The model has been run 100 times by randomizing the initial conditions for $\mathbf{x}$ and $\boldsymbol{\beta}$ within $\pm 10\%$ of the 2015 and 2016 passenger inflow counts per stations, after scaling the initial figures so that the sum is unit, as in Section 6. For each run, the highest 3, 15 and 30 stations (1%, 5% and 10% of the nodes, respectively) were given a unit score, and the scores were summed up by the line on which stations are. That is, if 2 of the most infected stations are on the same line, such a line gets a score 2. Likewise, if a station is amongst the most infected, all the lines passing through that station get a score 1. Over the 100 runs, this ranks the lines in the endemic case, where γ was calculated by randomly sampling $\mathcal{R}_\beta$ between 1 and 20. The excess journey time figures for 2014–15 and 2015–16 were compared to the ranking obtained from simulations, as described above, for the inflow of passengers recorded in 2015 and 2016, respectively. A proper validation of the model would require several of such comparisons. The one comparison shown here provides an indication that the model captures real system's features. Figs. A.1 and A.2 show in the first column the lines, indicated by their names, that have accumulated more delay in 2014–15 and 2015–16, in decreasing order. The second, third and forth columns are the rankings from the simulations. The heat map (same line, same colour) shows that the ranking does not change considerably, with cold-blue colours, representing lines with higher delays in the TFL data, consistently appearing on top of the ranking from simulations. In all cases bar one, three out of the first four more delayed lines are also present in the first 4 positions in the simulated results.

The Kendall-τ correlation coefficient (Kendall, 1938) has been calculated to quantify the change in ranking with respect to the TFL data. The coefficient measures the agreement of two rankings and it is calculated in a pairwise fashion comparing each of the rankings from the simulation results with the data available. The Kendall-τ correlation coefficient is positive when the two rankings are in agreement and unit when identical. It is negative when in disagreement, with -1 corresponding to the rankings being opposite. The values are reported at the bottom of the heat map in Figs. A.1 and A.2 together with the associated statistical significance through the p-value and show that all the rankings are in agreement. Finally, the nodes that more often are selected by the numerical simulations as showing a high infection tend are those at the intersection of more lines. Table A.1 shows the five stations that consistently show the five highest value of infection in the simulations. The p-value suggests that it is often not possible to discard the null hypothesis (here that the model does not capture the data). However, the small sample of only 10 aggregated data points would make it difficult to obtain low p-values if the null hypothesis was indeed false. Nevertheless, the positive Kendall-τ correlation coefficients confirm the model's ability to capture spreading of disruptions in transport networks.

Table A.1
Ranking of the stations from the more infected to the healthier for the 5 more infected stations from the 600 simulations performed. Stations tend to be amongst the most infected when at the intersection of more lines. The number of intersecting lines reported in the third column includes lines (e.g. Thameslink and DLR) for which delay data are not available and hence are not included in the line ranking.

Rank	Station name	Number of lines
1	Bank	4
2	King's Cross-St Pancras	7
3	Banker St	4
4	Green Park	3
5	Oxford Circus	4

References

Arim, M., Abades, S. R., Neill, P. E., Lima, M., & Marquet, P. A. (2006). Spread dynamics of invasive species. *Proceedings of the National Academy of Sciences, 103*(2), 374–378.

Bullo, F. (2019). *Lectures on network systems* (1st ed.).

Daley, D. J., & Kendall, D. G. (1965). Stochastic rumours. *IMA Journal of Applied Mathematics, 1*(1), 42–55.

De Domenico, M., Solé-Ribalta, A., Gómez, S., & Arenas, A. (2014). Navigability of interconnected networks under random failures. *Proceedings of the National Academy of Sciences*, *111*(23), 8351–8356.
Enright, J., & Kao, R. R. (2018). Epidemics on dynamic networks. *Epidemics*, *24*, 88–97.
Fall, A., Iggidr, A., Sallet, G., & Tewa, J. -J. (2007). Epidemiological models and Lyapunov functions. *Mathematical Modelling of Natural Phenomena*, *2*(1), 62–83.
Farina, L., & Rinaldi, S. (2000). *Positive linear systems: Theory and applications*. Wiley.
Garetto, M., Gong, W., & Towsley, D. (2003). Modeling malware spreading dynamics. In *IEEE INFOCOM 2003: Vol. 3* (pp. 1869-1879).
Gracy, S., Pare, P. E., Sandberg, H., & Johansson, K. H. (2020). Analysis and distributed control of periodic epidemic processes. *IEEE Transactions on Control of Network Systems*, 1, Online Early access.
Gutfraind, A. (2010). Optimizing topological cascade resilience based on the structure of terrorist networks. *PLoS One*, *5*(11).
Horn, R. A., & Johnson, C. R. (1990). *Matrix analysis*. Cambridge University Press.
Jacquez, J. A., & Simon, C. P. (1993). Qualitative theory of compartmental systems. *SIAM Review*, *35*(1), 43–79.
Kendall, M. G. (1938). A new measure of rank correlation. *Biometrika*, *30*(1–2), 81–93.
Khalil, H. K. (2002). *Nonlinear systems* (3rd ed.). Upper Saddle River, NJ: Prentice-Hall.
Khanafer, A., Başar, T., & Gharesifard, B. (2016). Stability of epidemic models over directed graphs: A positive systems approach. *Automatica*, *74*, 126–134.
Lajmanovich, A., & Yorke, J. A. (1976). A deterministic model for gonorrhea in a nonhomogeneous population. *Mathematical Biosciences*, *28*(3–4), 221–236.
Transport for London (2021). https://data.london.gov.uk/dataset/london-underground-performance-reports. (Accessed 26 June 2021).
Mager, D. E., & Jusko, W. J. (2001). General pharmacokinetic model for drugs exhibiting target-mediated drug disposition. *Journal of Pharmacokinetics and Pharmacodynamics*, *28*(6), 507–532.
Mei, W., Mohagheghi, S., Zampieri, S., & Bullo, F. (2017). On the dynamics of deterministic epidemic propagation over networks. *Annual Reviews in Control*, *44*, 116–128.
Meloni, S., Arenas, A., & Moreno, Y. (2009). Traffic-driven epidemic spreading in finite-size scale-free networks. *Proceedings of the National Academy of Sciences*, *106*(40), 16897–16902.
Mieghem, P. V., Omic, J., & Kooij, R. (2009). Virus spread in networks. *IEEE/ACM Transactions on Networking*, *17*(1), 1–14.
Nowzari, C., Preciado, V. M., & Pappas, G. J. (2016). Analysis and control of epidemics: A survey of spreading processes on complex networks. *IEEE Control Systems Magazine*, *36*(1), 26–46.
Pagliara, R., Dey, B., & Leonard, N. E. (2018). Bistability and resurgent epidemics in reinfection models. *IEEE Control Systems Letters*, *2*(2), 290–295.
Paré, P. E., Beck, C. L., & Nedić, A. (2018). Epidemic processes over time-varying networks. *IEEE Transactions on Control of Network Systems*, *5*(3), 1322–1334.
Pregnolato, M., Ford, A., Wilkinson, S. M., & Dawson, R. J. (2017). The impact of flooding on road transport: A depth-disruption function. *Transportation Research, Part D (Transport and Environment)*, *55*, 67–81.
Punzo, G., Young, G. F., Macdonald, M., & Leonard, N. E. (2016). Using network dynamical influence to drive consensus. *Scientific Reports*, *6*.
Rossi, R. A., & Ahmed, N. K. (2015). The network data repository with interactive graph analytics and visualization. In *AAAI*. http://networkrepository.com. (Accessed 26 June 2021).
Schäfer, B., Witthaut, D., Timme, M., & Latora, V. (2018). Dynamically induced cascading failures in power grids. *Nature Communications*, *9*(1), 1975.
Wu, Y., Pu, C., Li, L., & Zhang, G. (2019). Traffic-driven epidemic spreading and its control strategies. *Digital Communications and Networks*, *5*(1), 56–61, Artificial Intelligence for Future Wireless Communications and Networking.

Dr **Giuliano Punzo** graduated in aerospace engineering and briefly joined industry before his Ph.D. at the University of Strathclyde. Dr Punzo's interests span robotics, control theory, consensus and complexity. Dr Punzo joined the department of Automatic Controls and Systems Engineering at the University of Sheffield as a Lecturer in 2019, after post-doctoral appointments at the University of Glasgow, the University of Strathclyde and at the University of Sheffield.